ARMY RESEARCH LABORATORY

Gabor Jets for Clutter Rejection in Infrared Imagery

by Mark Wellman and Nasser Nasrabadi

ARL-TR-3400 **December 2004**

NOTICES

Disclaimers

Army Research Laboratory
Adelphi, MD 20783-1145

Gabor Jets for Clutter Rejection in Infrared Imagery

Mark Wellman and Nasser Nasrabadi
Sensors and Electron Devices Directorate, ARL

REPORT DOCUMENTATION PAGE

Form Approved OMB No. 0704-0188

1. REPORT DATE (DD-MM-YYYY)	2. REPORT TYPE	3. DATES COVERED (From - To)
December 2004	Final	08/03–04/04

4. TITLE AND SUBTITLE	5a. CONTRACT NUMBER
Gabor Jets for Clutter Rejection in Infrared Imagery	5b. GRANT NUMBER
	5c. PROGRAM ELEMENT NUMBER

6. AUTHOR(S)	5d. PROJECT NUMBER
Mark Wellman and Nasser Nasrabadi	5e. TASK NUMBER
	5f. WORK UNIT NUMBER

7. PERFORMING ORGANIZATION NAME(S) AND ADDRESS(ES)	8. PERFORMING ORGANIZATION REPORT NUMBER
U.S. Army Research Laboratory Sensors & Electron Devices Directorate (ATTN: AMSRD-ARL-SE-SE) mwellman@arl.army.mil Adelphi, MD 20783-1145	ARL-TR-3400

9. SPONSORING/MONITORING AGENCY NAME(S) AND ADDRESS(ES)	10. SPONSOR/MONITOR'S ACRONYM(S)
ARL 2800 Powder Mill Road Adelphi, MD 20783-1145	11. SPONSOR/MONITOR'S REPORT NUMBER(S)

12. DISTRIBUTION/AVAILABILITY STATEMENT

Approved for public release; distribution unlimited.

13. SUPPLEMENTARY NOTES

14. ABSTRACT

The performance of an infrared imagery based (IR) automatic target detection algorithm suffers from several variables. The target size, shape, orientation and brightness play a role, as well as the cluttered backgrounds [1-5], which often exhibit greater intensity than the sensor noise or intensity of the targets to be detected. Once the detection process is finished and further decisions pending in the ATR system, one would like a simple technique to further reduce false alarms. The problem again, is one of recognition and past research has shown that joint spatial-frequency representations using Gabor schemes is beneficial in many automated, computer vision applications. We will present results using Gabor Jets together with a back propagation neural network for a detector post processing procedure, which could substantially reduce false alarms.

15. SUBJECT TERMS Gabor, feature extraction, clutter rejection.

16. SECURITY CLASSIFICATION OF:			17. LIMITATION OF ABSTRACT	18. NUMBER OF PAGES	19a. NAME OF RESPONSIBLE PERSON
			UNCLASSIFIED	19	Heesung Kwon
a. REPORT	b. ABSTRACT	c. THIS PAGE			19b. TELEPHONE NUMBER (Include area code)
UNCLASSIFIED	UNCLASSIFIED	UNCLASSIFIED			(301) 394-1678

Standard Form 298 (Rev. 8/98)

Contents

Figures

This page is intentionally left blank.

1.   Introduction

D. Gabor recognized that the classical interpretation of images was limited in the sense that they were viewed as a collection of pixels (spatial domain) or a sum of sinusoids of infinite extent (spatial frequency domain). These were only the extremes of a joint spatial/frequency representation for an image where spatial frequency is considered a local phenomenon and varies with position in Gabors interpretation. The general form of the Gabor filters is given by Zhou [4] as;

$$\text{with} \quad u_0 = -\frac{2^{\frac{m}{2}}}{M} \cos(\frac{\pi n}{N}) \quad \text{and} \quad v_0 = -\frac{2^{\frac{m}{2}}}{M} \sin(\frac{\pi n}{N}) . \qquad (1)$$

Here we have M denoting the spatial dimension, m denoting the resolution level, N is the total number of orientations and n denotes the preferred orientation. The (x_0, y_0) is the position parameters which will localize the region in visual space.

The Gabor filter is optimized with respect to spatial-frequency representation. The proof of this can be found by considering that the 2-D Gabor filter is separable (eq (1)) and considering each 1-D counterpart, the 1-D Gabor filters achieves the minimal uncertainty product [6].

It's interesting that psychological and physiological studies present evidence of human and mammalian vision supporting some spatial-frequency analysis that maximizes the simultaneous localization of energy in both spatial and local frequency domains. The application of a suitable model like Gabor Jets in facial recognition is well motivated by the observation that some low level, spatial-frequency efficient processing is done at very early stages of development [7-8] and can account for size, shape and orientation discrimination. The argument is supported by indications of a large number of cells in the primary visual cortex, which are activated by the presence of a particular line or edge of specific orientation, size and position. [9] and are modeled by the "cortical receptive field profiles" or model which is a class of Gabor filters. For our application, Gabor Jets are simply a set of Gabor coefficients taken from one fixed image point with several points included in the overall set. This is a simplified form of the Gabor Jet procedure and will not require any elastic graph matching procedures used in facial recognition.

Another motivation for employing Gabor jets as a post processing clutter rejecter is attributed to the great deal of research in facial recognition, invariant shape recognition 4, directional feature extraction for perceptual grouping [10] and image retrieval [11]. Wiskot et al [12] employed Gabor Jets in a facial recognition task using fiducial points of the face, the pupils, corners of the mouth, tip of nose etc in creating labeled graphs. They further generalized these facial feature graphs to create a representative set of model graphs called a face bunch graph (FBG). The FBG lessoned the complexity and expense of covering a multitude of feature/facial combinations. We

site Wiskots [12] and Zhous [4] work due to the fact that a connection has been made to the low-level facial recognition abilities of a developing infant and Gabor representation as a suitable model for mammalian vision. We believe our machine vision task in delineating broadband, low-resolution IR imagery of target chips post detection may benefit from a Gabor application.

2.   Back Propagation

A simple and most often used architecture for discrimination is the back-propagation neural network (BPNN) which can allow for separation of complex hyperboundaries in feature space depending on the number and size of the hidden layers 12. We have employed the BPNN with an adaptive learning rate that allows fine-grain adjustments during training. Smoothing is also incorporated and allows the control of weight adjustment based on the past values of gradient descent and can prevent the training process from terminating in shallow local minimum. For class discrimination, the BPNN can provide both a robust classifier and a measure of your confidence in the classification decision. They derive their computational power from the parallel-distributed structure and the ability to learn and adapt. We trained our BPNN to a fixed 5% false alarm rate before testing and validation. False alarm rate is defined as the number of false alarms divided by the total number of clutter chips. Specifics governing the neural network training flow are beyond the scope of this paper. We will present several results using the BPNN for our clutter rejection task in later sections of the paper.

3.   Database for Clutter Rejection

The database consisted of over 20,000 target and clutter chips extracted manually from 10-bit gray scale FLIR imagery. A total of 10 targets were included in the database with chips being 40 × 75 pixels in size. Ground-truth information was used to center the silhouette for chip extraction at various viewing aspects. Chips termed "region of interest" or ROI were also used and were targets in less favorable conditions, i.e., near clutter or partially obscured. Figure 1 shows some examples of the various chips comparing the target and clutter set.
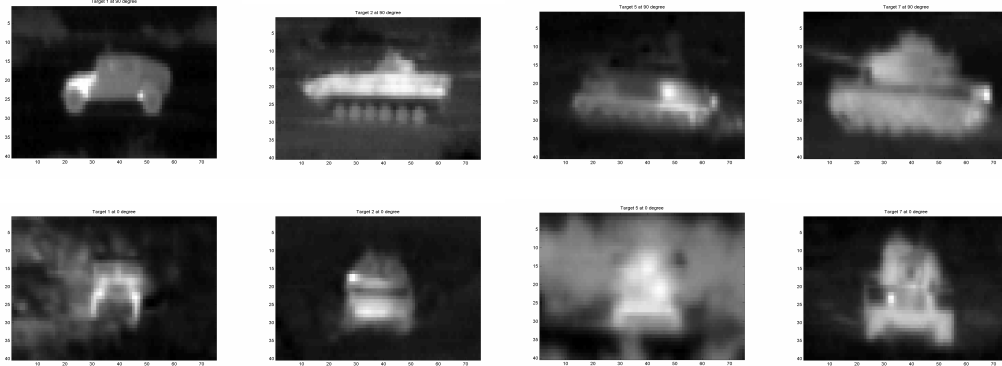
Above are examples of signature chips for some targets in the data set.
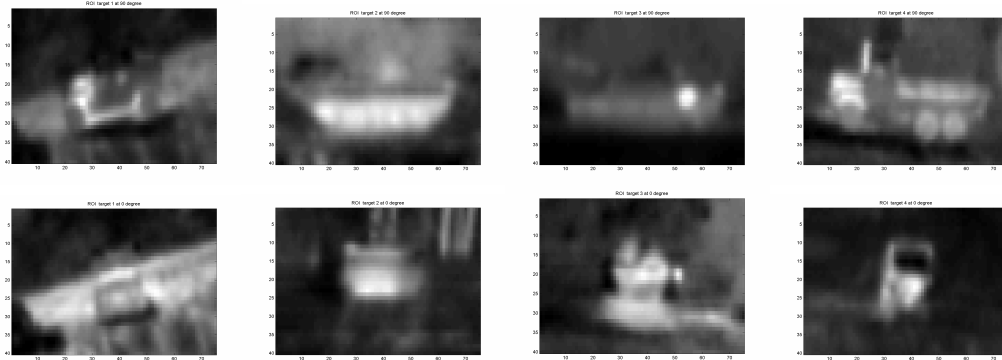
Above are examples of "Region of interest" chips.
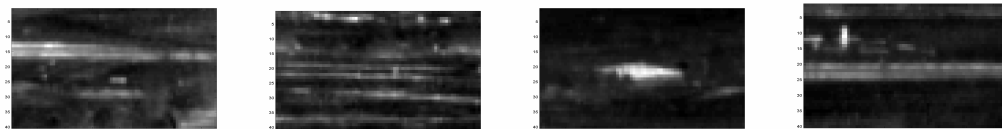
Above are examples of those clutter chips identified as targets by the ARTM detector.
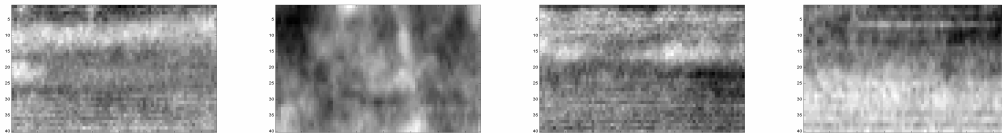
Above are examples of clutter chips.

Figure 1. Several examples of the various classes of chips considered in this research.

The target chips were extracted from the original input frame with the silhouettes centered within the chip and scaled to a constant range of 2 kilometers. This led to some chips being down-sampled and others being up-sampled form the original but the information of the chips remained relatively intact.

4. Procedure for Gabor Jets and Feature Vectors

Several Gabor Jet feature sets can be implemented in testing for clutter rejection which depends on ones choice of resolution levels and orientation. Examples of a symmetric and anti-symmetric Gabor filter are shown in figure 2. Preliminary experimentation results led to adopting Gaobr Jet feature set that included four resolution levels and six orientations. We found that employing more resolution levels and orientations gave no advantage and simpler sets like a Gabor Jet feature set consisting of 3 resolution levels with 4 orientations did not perform as well.

Figure 2. Example of symmetric and anti-symmetric Gabor filter.

For all Gabor features generated, we set the following relationship in equation 1:

$$\alpha = \beta \sim \frac{c}{\sigma} \ . \tag{2}$$

with c being a constant and σ, the standard deviation for the Gaussian in spatial domain x and y. This eliminates cross terms from equation 1.

The above relationship then allows the expression of the variance in x or y spatial domain to be;

$$\sigma^2 = M^2 \ 2^{-m} \ . \tag{3}$$

with the choice of constant $c = \pi$. We present results using 4 resolution levels and 6 orientations taken at 5 selected points of the image chip. Our selection of resolution levels is equivalent to 4 different variances for the Gabor filters with values of $2\sqrt{2}$, 2, $\sqrt{2}$ and 1.

Orientations at each resolution level are $0, \frac{\pi}{6}, \frac{\pi}{3}, \frac{\pi}{2}, \frac{2\pi}{3}$ and $\frac{5\pi}{6}$.

When considering the sample of 5 fixed points for each chip in the clutter rejection scheme, this will generate a feature vector of 120 features total. We will generate a standard feature set that is beneficial for the various sizes of targets. We will look at small, medium and elongated feature sets which are more size specific and an extended feature set that includes all size features.

The standard Gabor Jet feature set was used to train, test and validate a 120 by 60 by 2 BPNN. Hit rate for this BPNN architecture trained to 5% FAR was 90% post detection. Hit rate is defined as the number of target hits divided by the total number of target chips in the data set. Examples of the Gabor processed chips with the points used for standard Gabor jet marked in each image is shown in figure 3. We also created size specific trained BPNNs and fused their outputs as a second procedure using the standard set. See Table 1 in the result section for the results. Here we need to briefly mention how we selected size specific training, testing and validation sets. First, we employed the k-means 14 algorithm to determine the size of the silhouettes for various aspect angle of each target. Either signature (sig) or region of interest (roi) target silhouettes were used to generate specific sets for 3 BPNNs we called "small," "medium," and "elongated." We only used k-means to enable us to select the training set the 3 specific nets and not in determining the test and validation sets. K-means results were also utilized as a general guideline to determine the spatial placement for size specific features as seen in figure 4.
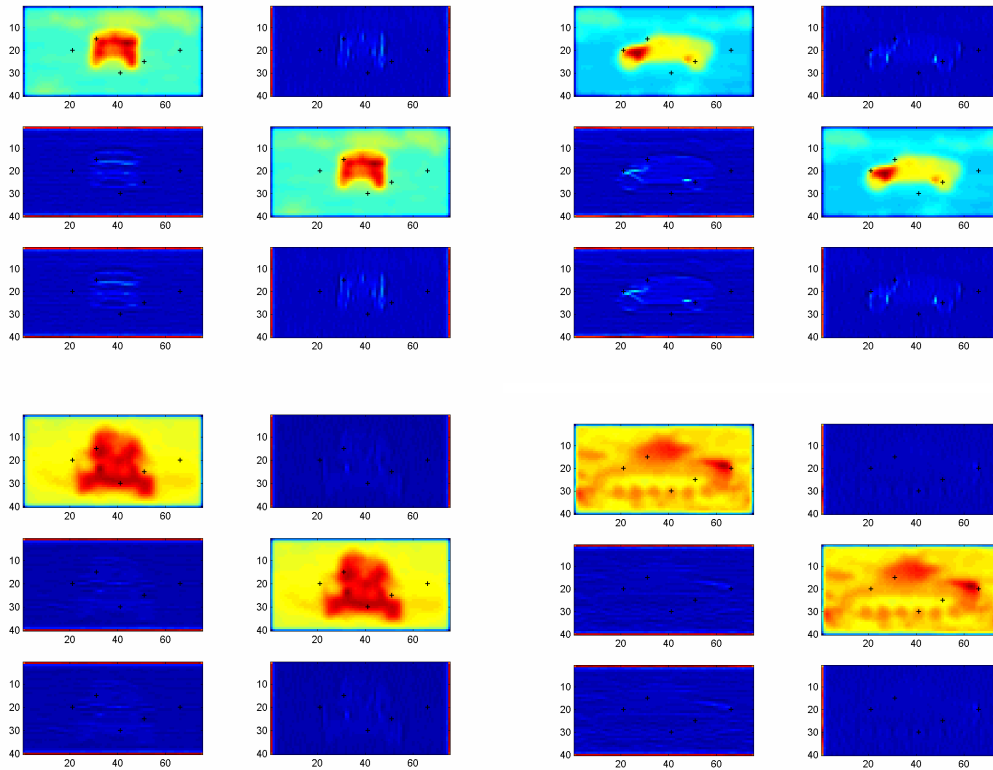

Figure 3. These are examples of the Gabor processed chips with the points used for standard Gabor jet marked in each image. Only 1 resolution level is shown for the 6 orientations.
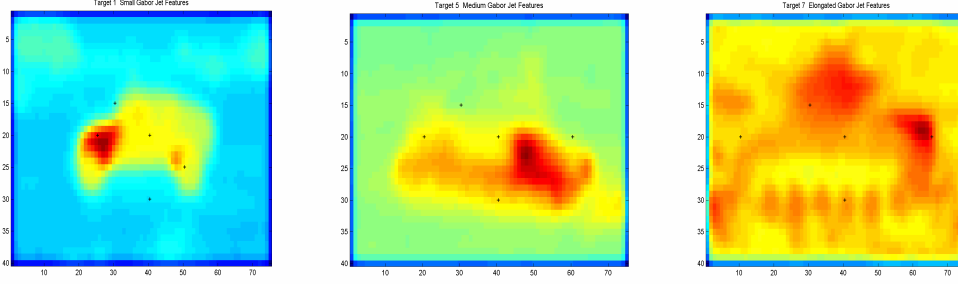
Figure 4. Small, medium and elongated Gabor jet processed images and the feature locations.

The K-means algorithm employs a measure based on the minimization of the sum of the squared distances from all points in a cluster domain to the cluster center.

The K-means procedure is as follows:

Step 1. Choose the initial K cluster centers $z_1(l),\ z_2(l),\ ....,z_K(l)$.

These are arbitrary and can be the first K samples of the data set.

Step 2. At the kth iteration, distribute the samples $\{x\}$ among the K cluster domains, using the relationship,

$$x \in S_j(k) \quad \text{if} \quad \left\| x - z_j(k) \right\| < \left\| x - z_i(k) \right\|$$

for all $i\ =\ 1,2,....,K,\ i \neq j,$ where $S_j(k)$ denotes the set of samples whose cluster center is $z_j(k)$. Ties can be resolved arbitrarily.

Step 3. From the result in step 2, compute the new cluster centers $z_j(\ k+1\ ),\ j=1,2,...,K,$ such that the sum of squared distances from all points in $S_j(k)$ to the new cluster center is minimized. Here, the new cluster center is computed so that the performance index

$$J_j = \sum_{x \in S_j(k)} \left\| x - z_j(k+1) \right\|^2,\ j=1,2,...,K$$

is minimized. This $z_j(k+1)$ that minimizes this performance index is the sample mean of $S_j(k)$. The new cluster center is given by

$$z_j(k+1) = \frac{1}{N_j} \sum_{x \in S_j(k)} x\ ,\ j=1,2,...,K \text{ where } N_j \text{ is the number of samples in } S_j(k).$$

Thus, the cluster centers are sequentially updated.

6

Step 4. If $z_j(k+1) = z_j(k)$ for $j = 1, 2, ..., K$, the algorithm has converged and the procedure is terminated. Otherwise, return to step 2.

Cluster results for the separation of the sig/roi sets into 3 clusters given as height, width were for small silhouettes 23, 36, for medium silhouettes 26, 54 and for elongated silhouettes 26, 64. Note that an elongated target can have a small silhouette when viewed head on or from behind or at angles close to these (0 and 180 degree). The silhouettes size were the basis for the separation procedure and not the physical size of the target. Figure 5 shows examples of the Full Gabor jet feature set combining small, medium and elongated features into a extended feature vector.
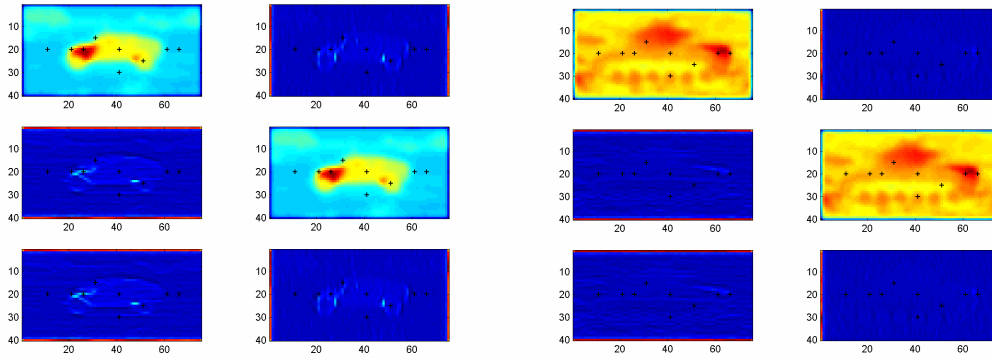
Figure 5. Examples of the Full Gabor jet feature set combining small, medium and elongated features into a extended feature vector.

Procedure for developing the BPNN of choice was "adhoc" in nature. We tried several differing architectures using either 1 or 2 hidden layers with a different numbers of hidden nodes in each layer. This led to a selection of a BPNN with 50% the number of hidden nodes compared to input nodes with only 1 hidden layer. A single hidden layer BPNN with this 50% rule performed better than BPNN with multiple hidden layers and is a very simple architecture.

5. Results

Table 1 has the results for each Gabor feature/BPNN experiment with the following paragraphs explaining each entry in detail. The experiments will be described briefly and given a corresponding tag for a table of results that list the test/validation scores.

The standard Gabor feature set was described earlier and the neural network architecture had 120 input nodes, 60 hidden nodes and 2 output nodes (120×60×2).

Table 1. Results of the 5 differing architectures and Gabor feature combinations where all BPNNs were trained to a 5% FAR rate before test and validation.

BPNN/Gabor	Hit Rate Test	Hit Rate Validation
STD	90%	91%
STD-SEG	88%	89%
SPC-SEG	91.7%	91%
SPC-ALL	95.5%	95.5%
STD-9	95.1%	96%

The BPNN was trained to a false alarm rate of 5% and the n hit rate was determined for the test and validation sets. The abbreviation for this result in table 1 is STD.

A standard set was developed for segmented size specific neural networks using the k-means analysis to segment the training database. Here we have 3 BPNN, each is $120 \times 60 \times 2$ and the output values were fused to determine the final result. Fusion and final scoring is done by taking the average or maximum value for the 3 clutter and target outputs associated with small, medium and elongated class neural nets. It was found that average or maximum gave the same result. The abbreviation for this result is STD-SEG in table 1.

A specific size dependent Gabor feature set was investigated where kmeans analysis allowed one to make a reasonable choice for the Gabor feature sets. Segmentation of the training data was also performed. Three BPNN were developed and final scoring was again done by fusing the neural net outputs. The abbreviation for this result is SPC-SEG in table 1.

A fourth experiment was to allow all the training data to be used for each size specific BPNN and size specific feature set. Here, we did not remove target silhouettes that were larger than the dedicated size specific feature set. For example, elongated target silhouettes were included in training the "small" NN with Gabor features chosen for small targets. Again, fusion of output results was performed and we use the abbreviation SPC-ALL in table 1 for the respective result.

The final result in table 1 is with one BPNN instead of using 3 size specific BPNN. Here, we looked at including all the size specific Gabor feature sets to train the single BPNN. This created a total of 216 feature inputs for the neural network and the architecture used was 216 by 108 by 2 using the 50% rule. There was no segmentation of training done in this case and the resulting Gabor feature vectors represent an expanded standard Gabor set. We abbreviate this in the table 1 as STD-9.

6. Conclusions

All indications conclude that the Gabor Jets features capture salient characteristics using this simplified approach. The standard sets performance was not improved when segmenting the training data based on size and this is due to the fact that often those chips which were certainly target and segmented as "medium" or "elongated" were now identified as clutter when presented to the "small" BPNN. "Elongated" target chips were to a lesser degree identified as clutter to the "medium" BPNN. When we introduced the size specific features and included segmented the training we had an improvement in hit rate over the standard set but only to a small degree. This is an interesting result since one would believe that the FAR for a "small" dedicated BPNN with size specific features would be affected in a similar manner as the standard set. For example, "elongated" targets being misclassified as clutter when presented to the "small" BPNN. The improvement over the standard set may be due to the fact that "small" silhouettes in test and validation are classified with higher confidence and therefore those "small" silhouettes originally misclassified are now correctly classified with no change to the misclassifications observed with the segmentation and standard set.   In removing all segmentation of the training data but having a dedicated BPNN for each size specific Gabor feature set gave considerable improvement. This architecture though is very complex considering you have 3 parallel BPNN's with a total of 360 features. The final result shows that the single BPNN can generalize 13 and perform as well as 3 separate BPNN and that the power of the clutter rejection lies in the features. This architecture is simpler requiring only 216 input nodes as opposed to 360 and 108 hidden nodes as opposed to 180.

Further work could involve using a procedure to estimate the silhouette size post detection and based on that estimate, determine which of the 3 size specific Gabor feature sets to use in the feature extraction. An interesting result would be to train the 3 size dedicated BPNN using a new rule developed from the automated measurement algorithm for the training silhouettes and subsequent k-means analysis. In fact, a preliminary "block and bound" procedure was used and after k-means clustering the resultant clusters were similar to k-means clusters for the "by hand" measurement of target silhouettes done in 1997 which we used in our experiments. Selecting 3 clusters for small, medium and elongated and using the "block and bound" procedure, the k-mean results were height, width for small 23, 48 , for medium 24, 56 and for elongated 24, 63. These clusters would be used to segment the training data base and provide a decision structure to determine the size specific Gabor feature set as each chip is addressed. Then, one would subject the test and validation data sets to the measurement procedure and in-turn pass the size specific Gabor features to the dedicated BPNN with final fusion of the output for scoring. This is a complex procedure though and even if the result gains a ½ % in clutter rejection, one would doubt that it is more beneficial than the STD-9 approach.

7. Bibliography

1. A. Aridgides, M. Fernanadez, D. Randolph, D. Bray , "Adaptive Three-Dimensional Spatio-Temporal Filtering Techniques for Infrared Clutter Suppression," SPIE Vol. 1305 Signal and Data processing of Small Targets, 1990 pp 63-74.

2. T. Meitzler, G. Gerhart, E. Sohn, H. Sigh, "Detection Probability Using Relative Clutter in Infrared Images," IEEE Transactions on Aerospace and Electronic Systems, Vol. 34, No. 3 July 1998 , pp 955-961.

3. S. Der, C. Dwan, A. Chan, H. Kwon and N.M. Nasrabadi, "Scale-Insensitive Detection Algorithm for FLIR Imagery," Army Research Laboratory technical report, ARL-TN-175, February 2001.

4. Y. T. Zhou, R. Crenshaw, "Contrast, Size and orientation Invariant Target Detection in Infrared Imagery," SPIE Vol. 1471 Automatic Object Recognition, 1991 pp 404-411.

5. A. Tartakovsky, R. Blazek, "Effective Adaptive Spatial-Temporal Technique for Clutter Rejection in IRST," SPIE Vol. 4048 Siganl and Data processing of Small Targets, 2000.

6. R. Bracewell, "The Fourier Transform and Its Applications," Second Edition, McGraw-Hill Book Company, 1986.

7. M. Turk, A. Pentland, "Face Recognition using eigenfaces," Proc. IEEE Computer Society Conf. Computer Vision and Pattern Recognition (Maui, HI), June 1991, pp. 586-591.

8. J. D. Daugman, "Uncertainty relations for resolution in space, spatial frequency, and orientation optimized by two-dimensional visual cortex filters," J. Opt. Soc. Am. A, Vol. 2, no. 7, 1985, pp. 1160-1169.

9. P. Laplante, A. Stoyenko, "Real-Time Imaging Theory, Techniques, and Applications," IEEE Press, Piscataway, NJ.

10. M. Carriera, M. Mirmedhi, B. Thomas, J. Haddon, "Grouping of Directional Features using a Extended Hough Transform," Proc. 15th International Conference on Pattern Recognition 2000, Barcelona, Spain, vol. 3, pp. 990-993.

11. B. Manjunath, W. Ma, "Texture features for browsing and retrieval of large image data," IEEE Trans on Pattern Analysis and Machine Intelligence, Vol. 18 (8), August 1996, pp. 837-842.

12. L. Wiskot, J. Fellous, N. Kruger. C. Malsburg," Face Recognition by Elastic Bunch Graph Matching," IEEE Trans on Pattern Analysis and Machine Intelligence, Vol. 19, No. 7, July 1997 pp.775-779.

13. S. Haykin, "Neural Networks, A Comprehensive Foundation," Macmillan Publishing Company, New Jersey, 1994.

14. K. Fukunaga, "Introduction to Statistical Pattern Recognition," 2nd Edition Academic Press, San Diego, 1990.

Distribution List

Admnstr
Defns Techl Info Ctr
ATTN DTIC-OCP (Electronic copy)
8725 John J Kingman Rd Ste 0944
FT Belvoir VA 22060-6218

DARPA
ATTN C Schwartz
ATTN IXO S Welby
ATTN R Hummell
3701 N Fairfax Dr
Arlington VA 22203-1714

Ofc of the Secy of Defns
ATTN ODDRE (R&AT)
The Pentagon
Washington DC 20301-3080

US Army RDECOM AMRDEC
ATTN ATCD-B
FT Monroe VA 23651-5850

Army Rsrch Physics Div
ATTN AMSRD-ARL-RO-MM   R Launer
PO Box 12211
Research Triangle Park NC 27709-2211

US Army TRADOC
Battle Lab Integration & Techl Dirctrt
ATTN ATCH-B
10 Whistler Lane
FT Monroe VA 23651-5850

CECOM NVESD
ATTN AMSRD-CER-NV-D J Ratches
10221 Burbeck Rd Ste 430
FT Belvoir VA 22060-5806

US Army Aberdeen Test Center
ATTN CSTE-DT-AT-WC-A F Carlen
400 Colleran Road
Aberdeen Proving Ground MD 21005-5009

US Army Aberdeen Test Center
ATTN CSTE-DTC-AT-TC-N D L Jennings
400 Colleran Road
Aberdeen Proving Ground MD 21005-5059

US Army Aviation & Mis Lab
ATTN AMSRD-AMR-SG-IP H F
Anderson
Bldg 5400
Redstone Arsenal AL 35809

US Army CERDEC, NVESD
ATTN AMSRD-CER-NV-xx J Hilger
ATTN AMSRD-CER-NV-xx P Perconti
ATTN AMSRD-CER-NV-xx R Driggers
10221 Burbeck Rd Ste 430
FT Belvoir VA 22060-5806

US Army ERDC
ATTN CEERD-TR-S R Rand
7701 Telegraph Rd
Bldg 2592
Alexandria VA 22315

US Army Materiel Sys Anal Actvty
ATTN AMSRD-AMS-SC E Grove
392 Hopkins Rd
Aberdeen Proving Ground MD 21005-5071

US Army Materiel Sys Anal Actvty
ATTN AMSRD-AMS-SC G Kistner
Aberdeen Proving Ground MD 21005-5071

US Army Materiel Sys Anal Actvty
ATTN AMSRD-AMS-SC J Mazz
392 Hopkins Rd
Aberdeen Proving Ground MD 21005-5071

US Army Natick RDEC
Acting Techl Dir
ATTN SBCN-TP P Brandler
Kansas Street Bldg 78
Natick MA 01760-5056

US Army PM NV/RSTA
ATTN SFAE-IEW&S-NV D Ferrett
10221 Burbeck Rd
FT Belvoir VA 22060-5806

US Army RDECOM AMRDEC
ATTN ATCD-B
FT Monroe VA 23651-5850

US Army RDECOM AMRDEC
ATTN AMSRD-AMR-SG-IP R Sims
Bldg 5400
Redstone Arsenal AL 35898

US Army RDECOM AMRDEC
ATTN AMSRD-AMR-WS-PL W
Davenport
Bldg 7804
Redstone Arsenal AL 35898

Commanding General
US Army RDECOM AMRDEC
ATTN AMSRD-AMR W C McCorkle
Bldg 5400
Redstone Arsenal AL 35898-5000

US Army RDECOM ARDEC
ATTN AMSRD-AAR-QES P Willson
Radiographic Laboratory, B.908
Picatinney Arsenal NJ 07806-5000

US Army RDECOM ARDEC
ATTN AMSTA-AR-TD
Bldg 1
Picatinny Arsenal NJ 07806-5000

US Army RDECOM TARDEC
ATTN AMSRD-TAR-R G R Gerhart
MS 263
Warren MI 48397-5000

US Army Soldier & Biological Chem Ctr
ATTN AMSSB-RRT-DP W Loerop
Edgewood Chem & Biological Ctr
Bldg E-5554
Aberdeen Proving Ground MD 21010-5424

Commander
USAISEC
ATTN AMSEL-TD   Blau
Building 61801
FT Huachuca AZ 85613-5300

AFRL/SNAA
ATTN M Jarratt
2241 avionics Circle Area B, Bldg 620
Wright Patterson AFB OH 45433-7321

CMTCO
ATTN MAJ A Suzuki
1030 S Highway A1A
Patrick AFB FL 23925-3002

SITAC
ATTN H Stiles
ATTN K White
ATTN R Downie
11981 Lee Jackson Memorial Hwy Suite 500
Fairfax VA 22033-3309

US Army Rsrch Lab
ATTN AMSRD-ARL-WM-BF G Haas
ATTN AMSRD-ARL-WM-BF W Oberle
Aberdeen Proving Ground MD 21005-5067

Director
US Army Rsrch Lab
ATTN AMSRD-ARL-RO-D JCI Chang
PO Box 12211
Research Triangle Park NC 27709

US Army Rsrch Lab
ATTN AMSRD-ARL-RO-EL W Sander
PO Box 12211
Research Triangle Park NC 27709-2211

US Army Rsrch Office
ATTN AMSRD-ARL-RO-PP R Hammond
PO box 12211
Research Triangle Park NC 27709-2211

US Army Rsrch Lab
ATTN AMSRD-ARL-CI-OK-T Techl Pub
(2 copies)
ATTN AMSRD-ARL-CI-OK-TL Techl Lib
(2 CD's)
ATTN AMSRD-ARL-D A Grum

ATTN AMSRD-ARL-D J M Miller
ATTN AMSRD-ARL-SE J Pellegrino
ATTN AMSRD-ARL-SE J Rocchio
ATTN AMSRD-ARL-SE-S J Eicke
ATTN AMSRD-ARL-SE-SE N Nasrabadi
ATTN AMSRD-ARL-SE-SE P Gillespie
ATTN IMNE-AD-IM-DR Mail & Records
Mgmt (1 CD)
ATTN AMSRD-ARL-SE-SE H Kwon